

Enabling Visual Composition and Animation in Unsupervised Video Generation

Aram Davtyan¹, Sepehr Sameni¹, Björn Ommer², and Paolo Favaro¹

¹ Computer Vision Group, Institute of Informatics, University of Bern, Switzerland

² CompVis @ LMU Munich and MCML, Germany

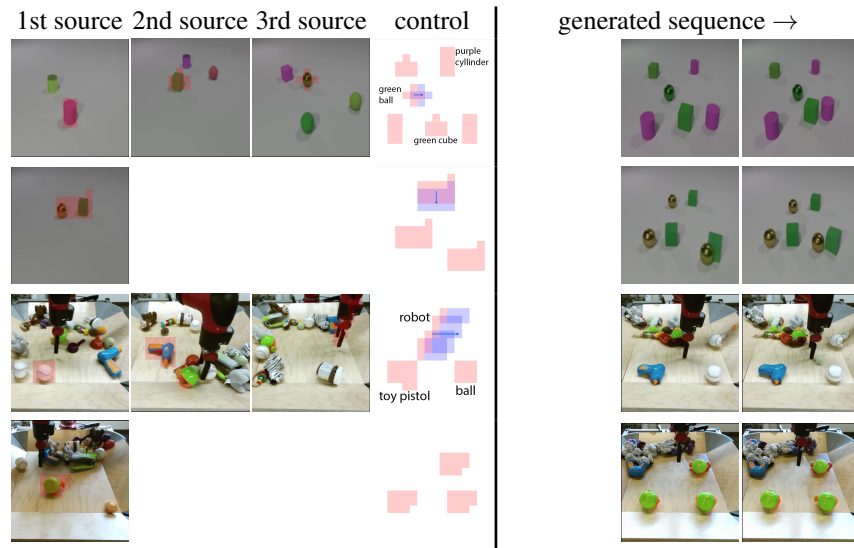


Fig. 1: Scene composition and animation with CAGE on the CLEVRER and the BAIR datasets. CAGE is able to combine multiple object features from different source images and use them to compose and animate the scene in a controllable way. The selected features are shown as overlaying red patches. Blue patches in the controls correspond to the intended future locations of the objects. Notice the ability of the model to carefully adjust the appearances (e.g. sizes, shadows and lights) of the objects based on their location in the target layout. Click on the first images in the generated sequences to play them as videos in Acrobat Reader.

Abstract. In this work we propose a novel method for unsupervised controllable video generation. Once trained on a dataset of unannotated videos, at inference our model is capable of both composing scenes of predefined object parts and animating them in a plausible and controlled way. This is achieved by conditioning video generation on a randomly selected subset of local pre-trained self-supervised features during training. We call our model CAGE for visual Composition and Animation for video Generation. We conduct a series of experiments to demonstrate capabilities of CAGE in various settings. Project website: <https://araachie.github.io/cage>.

Keywords: Controllable Video Generation · Scene Generation · Unsupervised Learning

1 Introduction

Simulators play a crucial role in training and evaluating intelligent agents across various domains, such as robotics [23], autonomous driving³ [26, 36, 57, 76], and video games [41]. These simulators allow to design virtual environments where agents can interact and learn. This allows for rapid testing of different algorithms and planning strategies. Moreover, simulators enable the exploration of object interactions that are challenging or unsafe to replicate in the real world, such as collisions.

Although physics simulators, like Isaac Gym [51], can be highly versatile, they may lack the realism required for complex real-world scenarios where object interactions are intricate. Furthermore, designing synthetic environments demands significant human effort, limiting the scalability of these tools.

To bridge this gap, there has been a growing effort on constructing “world models” [25, 43]. These models are trained directly on real videos and, in their simplest form, predict future observations based on past ones. A notable feature of these models is their controllability, enabling users to specify desired changes in the environment—such as specific actions (e.g., moving the agent in a certain direction)—and simulate the outcomes. However, integrating this capability presents challenges due to the unavailability of information about ongoing actions in the environment: While an agent may have access to its ego-motion, it typically lacks knowledge of other objects’ motion in the scene. To address this limitation, recent advancements have proposed unsupervised learning methods that build controllable world models only from real videos (*i.e.*, without any information about the actions or the action space) [4, 5, 15, 53]. In these models, control is often defined as a separate input from visual data, ranging from motion encodings [4, 15] to general feature embeddings [5, 52, 53], which are learned directly from the visual data. However, these control signal choices impose limitations on the tasks the world model can perform (*e.g.*, they allow to specify objects’ motion, but not how to compose a scene), which we aim to address in this work.

We propose CAGE, short for *visual Composition and Animation for video GEneration*, a generative model capable of creating environments and animating objects within them (see Fig. 1). A key innovation in CAGE is that its control is specified directly through a set of “visual tokens” rather than embeddings from a separate action space. These visual tokens provide information regarding the identity of objects (*what*), or parts thereof, and their spatio-temporal placement provides information about *where* the objects should appear in certain frames in the future. As visual tokens we use DINOv2 spatial features [56]. Our experiments demonstrate that leveraging DINOv2 features enables our model to mitigate overfitting to the control signal and facilitates zero-shot transfer from other image domains. During training, we extract DINOv2 features from future video frames and utilize a sparse subset of these features as the control signal. By using this partial information, the world model is trained to inpaint the surrounding context, both spatially and temporally, and thus learns to generate future frames consistent with the specified control signal. In summary, CAGE produces a video output that encapsulates the desired composite scene, along with animations depicting the ob-

³ For example, GAIA by Wayve (<https://wayve.ai>) and the world models developed by Waabi (<https://waabi.ai>)

jects within it, including their interactions. Given that CAGE solely employs videos as training data, it undergoes entirely unsupervised training and can be readily scaled to accommodate large datasets. Our main contributions are summarized as follows:

- CAGE introduces a novel controllable video generation model capable of scene creation through composition and of object animation;
- we introduce a unified control format that simultaneously can specify how to compose and animate a scene through a sparse set of visual tokens. This format allows to describe a wider range of prediction tasks than motion-based controls. In particular, it allows to compose scenes. Moreover, our control allows zero-shot transfer from frames not in our training set;
- in comparison to prior work, the realism of videos generated through CAGE is higher (according to the metrics commonly used in the literature) and the controllability of our control format is established through a set of experiments.

2 Prior Work

We briefly summarize prior work related to CAGE and highlight the advantages and disadvantages of different conditioning approaches.

Video Generation. Recent advancements in the field of video generation have been remarkable, driven predominantly by the impressive capabilities of diffusion models. These models have significantly enhanced the generation of both images and videos from text descriptions, setting a new benchmark in the domain. The foundational work in text-to-image generation [18, 32, 58, 61] has laid the groundwork for these advancements, paving the way for their extension into the text-to-video arena [24, 31, 34]. This has resulted in the production of high-definition, high-resolution, and fluid videos. However, as highlighted by Blattmann *et al.* [3] and Zhang *et al.* [75], despite these advancements, current text-to-video models often produce videos with objects whose motion trajectories appear relatively random. Moreover, specifying precise motion dynamics with a lone text prompt poses significant challenges.

Supervised Controllable Video Generation. A first approach that can exploit more accurate motion specifications in the text prompt is MAGE [38]. This approach aligns well with the text-to-video generation pipeline, albeit necessitating increased supervision. An alternative strategy is to use ControlNet [77] for videos [11, 50, 79]. This is particularly effective when the future frame structure is known, as it offers a predefined control mechanism. Additionally, there are models designed to condition on both of these controls [74], resulting in a versatile framework for guided video generation. In an effort to reduce the reliance on extensive supervision, models such as Boximator [68], Motion-I2V [60], and Motion-Zero [9] have emerged. These models enhance motion generation’s controllability and user guidance by employing bounding boxes or motion flows as more intuitive control mechanisms. Boximator, in particular, represents a significant leap forward, enabling precise control over object positions and trajectories through constraint-based modeling. Motion-I2V introduces a two-stage image-to-video mapping process, incorporating explicit motion modeling to achieve consistent and controllable video generation. Motion-Zero further advances the field by proposing a zero-shot control framework to define the trajectory of moving objects. These

models rely on supervised learning paradigms and in particular on text descriptions. While effective, this reliance poses inherent limitations on scalability and adaptability, as supervised methods require large, labeled datasets, which are resource-intensive to produce and may reduce their applicability scope.

Unsupervised Controllable Video Generation. Unsupervised approaches in video generation have been gaining traction, primarily focusing on leveraging implicit signals such as flow vectors [2, 16, 27], masks [40], and learned actions [5, 53]. These methods offer a promising avenue by minimizing reliance on extensive labeled datasets, thus addressing the scalability and adaptability challenges inherent in supervised models. Recent innovations in diffusion models and conditional flow matching [46, 47] have further bolstered unsupervised video generation capabilities [17, 35, 67]. However, despite the steep progress, these models often struggle with achieving cross-scene generalization, as their generative capabilities are tightly coupled with the specificity of the conditioning signals used during training.

Latent Conditioned Image Generation. The domain of unsupervised image generation has similarly witnessed considerable progress, greatly propelled by advancements in diffusion models and the innovative use of self-supervised features for conditioning. Techniques for global conditioning have made strides, employing consistency-based image representation learners [6, 7, 10, 12, 55, 56] to generate coherent and generalizable representations of objects and scenes [8, 37, 45]. These global features offer a robust foundation for conditional generative models, facilitating a higher level of scene understanding and object representation. On the local conditioning front, techniques like Masked Autoencoders [29] can be used to manipulate scene composition through object movement [1] and inpainting. However, these methods are not trained to be robust to changes in object properties relative to their new positions, such as scale, shadows, and lighting, and thus present a limitation in achieving realistic scene dynamics.

Building upon these insights, our model introduces an innovative approach by leveraging sparse DINOv2 [56] spatial features for local conditioning in video generation. This methodology not only simplifies the process of scene composition and object animation but also addresses the challenge of maintaining realistic object properties across different scene contexts. By combining the strengths of unsupervised learning with intuitive and flexible control mechanisms, our model represents a significant step forward in the field of video generation. In the following section, we will delve deeper into the specifics of our approach, outlining the technical framework and demonstrating its efficacy through experimental results.

3 Inside the CAGE

The goal of controllable video generation is to learn the following conditional distribution

$$p(x^{n+1:n+k} \mid x^{1:n}, a^{n+1:n+k}), \quad (1)$$

where $x^i \in \mathbb{R}^{3 \times H \times W}$, $i = 1, \dots, n + k$ is a sequence of RGB video frames, a^i is the control at time i , and $x^{i:j}$ ($a^{i:j}$) denotes the set of consecutive video frames (controls) between times i and $j \geq i$. Following [17] we model the distribution in

eq. (1) as a denoising process in the conditional flow matching (CFM) formulation of diffusion [46]. In CFM, the model $v_t(x_t^{n+1:n+k} | x^{1:n}, a^{n+1:n+k}, \theta)$ with parameters θ is trained to approximate the direction of the straight line that connects independently sampled noise and data points:

$$\theta^* = \arg \min_{\theta} \mathbb{E}_{t, x_0, x_1, a} \|v_t - x_1^{n+1:n+k} + (1 - \sigma_m)x_0^{n+1:n+k}\|_2^2. \quad (2)$$

Here t is a random timestamp sampled from $U[0, 1]$, $x_0^i \sim \mathcal{N}(0, I)$, $x^{1:n+k}$ and $a^{n+1:n+k}$ are sampled from the dataset, and $x_t^i = tx^i + (1 - (1 - \sigma_m)t)x_0^i$ with a small $\sigma_m \approx 10^{-7}$. It can be shown that integrating from $t = 0$ to $t = 1$ the following ODE

$$\begin{aligned} \dot{X}_t &= v_t(X_t | x^{1:n}, a^{n+1:n+k}, \theta^*), \\ p(X_0) &= \mathcal{N}(0, I), \end{aligned} \quad (3)$$

where X_t denotes the window of noisy future frames $x_t^{n+1:n+k}$, leads to $p(X_1) \approx p(x^{n+1:n+k} | x^{1:n}, a^{n+1:n+k})$. That is, to sample from the probability density function in eq. (1) one can sample Gaussian noise at time 0 and gradually denoise it by following the trajectories of eq. (3) till time $t = 1$. For more details, please refer to [46].

As suggested in [17] we relax the computational complexity of conditioning on the past frames by distributing the conditioning over the flow integration steps. This allows to effectively condition each step only on two past observations: the previous one x^n (the reference) and one uniformly sampled from the past x^c (the context). Thus, we work with the model $v_t(x_t^{n+1:n+k} | x^n, x^c, a^{n+1:n+k}, \theta)$, $c \sim U\{1, \dots, n - 1\}$. At inference, c is also randomized at each integration step of the ODE. This allows the model to observe all the past frames, while keeping the computational costs constant.

We also observed that decoupling the noise levels of separate frames during training is beneficial to the quality of the generated frames. *I.e.*, we set $t = (t_1, \dots, t_k)$ with independently sampled t_i that are not necessarily equal to each other and $X_t = x_t^{n+1:n+k} = (x_{t_1}^{n+1}, \dots, x_{t_k}^{n+k})$. This allows the noisy frames to exploit shared information (*e.g.*, the background) in the less noisy frames and leads to improved training. Besides this, the model with decoupled t is more flexible at inference, where the denoising can be done within a sliding window of monotonously growing noise levels. However, here we do not investigate this further and instead focus on the model’s controllability. A similar technique was proposed for motion synthesis [80] and concurrently for video diffusion [59].

Lastly, before we proceed to the definition of our control format, we would like to point out an important requirement for our model. To enable the synthesis of a scene given only the controls (also referred to as “from scratch”), we drop the conditioning on the context frame for 50% of the training. Moreover, we drop the reference frame 20% of the time during which we drop the context frame. By simultaneously training our model under different conditioning settings, we endow it with the ability to both predict videos from some initial frames and to generate them from scratch.

3.1 Controlling Scene Composition over Time via Sparse Features

Our goal is to build a video generation model in which the controls can serve both as motion guidance for the video prior and as scene generation specifications. The lat-

ter control means that when we omit the conditioning on the past, the model has to generate and animate the scene from scratch. The control input describes the scene in terms of objects (or parts thereof) and their positions in space and time. In contrast to prior work that is either limited to only scene generation [21, 42, 54] or uses supervision [39, 49], instead of leveraging composite separate solutions for scene generation and animation [5, 68], we seek for a unified control that can simultaneously solve both problems in an unsupervised way.

To this end, we propose to use a sparse set of DINOv2 [56] spatial tokens from the last l ViT [19] layers as the controls a^i . More precisely, for each future frame x^i , each spatial token from the 16×16 grid $f^i \in \mathbb{R}^{d \times 16 \times 16}$ of its DINOv2 encodings is assigned a probability $\pi \in [0, 1]$ to be selected for control. Then, a random 16×16 mask $m^i \in \mathbb{R}^{16 \times 16}$ is sampled from the corresponding Bernoulli distribution. This mask consists of 0s and 1s, where 1s stand for the selected tokens. The control is then calculated as

$$a = m \cdot f + (1 - m) \cdot [\text{MSK}], \quad (4)$$

where $[\text{MSK}] \in \mathbb{R}^{d \times 1 \times 1}$ is a trainable token (upper indices are omitted for simplicity).

By conditioning on sparse DINOv2 features and training for video prediction (generation) we rely on two major advantages of this control. 1) The controls are unified and data-agnostic. Meaning that at test-time the scene can be composed of objects from different images (even other domain to a certain extent, which we demonstrate later) by adopting their DINOv2 features. And the motion can be specified by changing the position of the features in the future frames. 2) The controls are abstract enough to actually allow for moving objects from their original locations and changing their appearances accordingly, while keeping the features the same. In contrast, if one used pixel patches as controls, the model could have overfitted to the texture information in the pixels to recover the position of the patch. Indeed, we show in the ablations that the controllability suffers from too much information about the underlying patches in the controls. By default, unless otherwise stated, we leverage the ViT-S/14 version of DINOv2.

3.2 Scale and Position Invariance

Even though the DINOv2 features are quite abstract they have one major issue, which is the fact that they preserve too much information about the original position of the patches in an image [71, 72]. Thus, naively conditioning on those features would lead to overfitting to the internal positional information and hence to limited controllability over the locations of the objects (see Sec. 4.2 and Fig. 4). In order to mitigate this issue, we propose to distort the features in such a way that would keep the identities of the objects, but would destroy the position information. To do so, we calculate the features on random crops instead of whole images. This way the position of the objects within the crop always changes during the training, which makes the model ignore that information. This procedure is illustrated in Fig. 3.

3.3 Out of Distribution Controls

Prior work, namely YODA [16], has demonstrated remarkable capabilities of generalizing to out of distribution (o.o.d.) control. For instance, with YODA, one is able to move

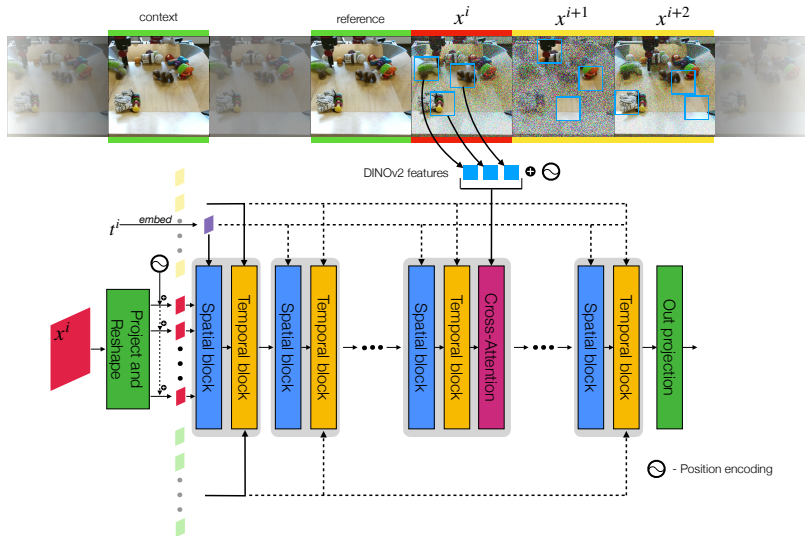


Fig. 2: Overall pipeline of CAGE. The model takes all the colored frames and processes them equally and in parallel. The pipeline for a single frame (x^i , in red) is illustrated. CAGE is trained to predict the denoising direction for the future frames ($x^{i:i+2}$) in the CFM [46] framework conditioned on the past frames (*context* and *reference*) and sparse random sets of DINOv2 [56] features. The frames communicate with each other via the Temporal Blocks while being separately processed by the Spatial Blocks. The controls are incorporated through Cross-Attention.

the background objects in the BAIR [20] dataset. In the training set, those only move when pushed by the robotic arm. This is achieved by balancing two things during the training: 1) the learning of the video prior (how things should move if no controls are specified) and 2) the learning to follow the controls. The right balance is the outcome of tuning many components, among which the most important ones, according to the authors of [16], are the number of the controls and where they are sampled. In contrast, we propose to keep the training simple and rely on the compositionality. Our method has no restrictions on where the controls can be sampled from. Instead, we propose to find the balance at test time by utilizing classifier-free guidance [33] to allow generalization to the o.o.d. controls. More precisely, we modify the estimated vector field with

$$v_t = (1 + w) \cdot v_t(X_t | x^{1:n}, a^{n+1:n+k}, \theta^*) - w \cdot v_t(X_t | x^{1:n}, \emptyset, \theta^*), \quad (5)$$

where $w \geq 0$ is the guidance strength. The larger w the more the model relies on the control (to move background objects) rather than on the video prior (not to move background objects). Figure 5 shows some examples of o.o.d. controls in BAIR.

3.4 Training Details and Architecture

For computational efficiency, as proposed in [58], CAGE works in the latent space of a pre-trained VQGAN [22]. All frames $x^{n:n+k}$ as well as x^c are separately encoded to

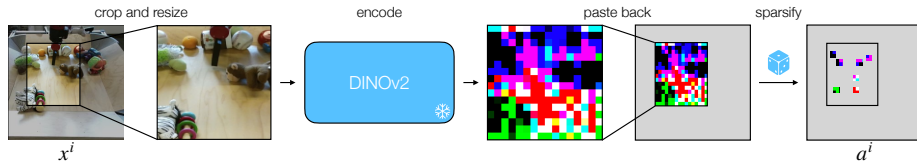


Fig. 3: The process of selecting controls for conditioning. The image is first cropped and resized to 224×224 resolution that can be fed to DINOv2 to obtain the spatial tokens. Those are then pasted back to the original location of the crop and sparsified. This is done to prevent overfitting to the position information that is present in DINOv2 features. Besides this, calculating the features on the crops of the image makes the model scale invariant. That is, at inference we are able to copy objects from the background and paste them to the foreground and vice versa. The model should be able to automatically figure out how to scale the objects according to their target position in the scene as well as how to add other position-related textures (e.g. shadows).

latents. Each latent is a feature map of shape $c \times h \times w$. These latents are first reshaped to $(h \cdot w) \times c$. Then a random set of tokens (but the same across time [63]) is dropped from each of the latent codes, leaving $m = \lfloor (1 - r) \cdot h \cdot w \rfloor$ tokens per latent. Here r is the masking ratio that is typically equal to 0.4 in our experiments. The remaining tokens are then concatenated in the first dimension to form a single sequence of $(k + 2) \cdot m$ tokens. This sequence is then passed to v_t , which we model as a Transformer [66] that consists of 9 blocks of alternating spatial and temporal attention layers. Spatial layers are allowed to only attend to the tokens within a given frame, while temporal layers observe all the tokens. As suggested in [28], t is embedded in the architecture as a time-dependent bias that is added to the queries, keys and values in all attention layers. We add learnable spatial position encodings to all the tokens before feeding them to v_t . The same position encodings are later added to the control tokens $a^{n+1:n+k}$. For the video indices temporal layers employ relative position encodings [70]. 5 middle blocks of the Transformer additionally incorporate cross-attention layers, where tokens from the i -th frame attend to a^i . The overall pipeline of CAGE is depicted in Fig. 2.

All models except for the ablations are trained for 100k iterations with batch size 64 distributed across 4 Nvidia RTX 3090 GPUs. The models for the ablations are trained on a single GPU with batch size 16. All models are trained in mixed-precision (fp16) using AdamW [48] optimizer with the square root learning rate schedule with the largest learning rate equal to $1e-4$ and 5k warmup steps. Weight decay of $5e-6$ is used.

4 Experiments

In this section we conduct a series of experiments on several datasets to highlight different capabilities of CAGE and demonstrate its superiority over the prior work.

4.1 Data

We test our model on 3 datasets. Ablations are conducted on the **CLEVRER** [73] dataset. This dataset consists of 10k training videos capturing multiple synthetic objects colliding into each other and interacting on a flat surface. This dataset combines

simplicity of the objects with quite interesting interactions and supports compositionality making it a great field for experimentation. We further test CAGE on the **BAIR** [20] dataset, which is a dataset containing 44k clips of a real robotic arm manipulating diverse set of objects on a table. This dataset provides more complex objects and interactions and is suitable for demonstrating generalization to o.o.d. controls. Finally, we test our model on real egocentric videos from the **EPIC-KITCHENS** [13] dataset. For making the training more resource efficient, we restrict ourselves to a single person/kitchen from the dataset, namely P03.

4.2 Ablations

We start by ablating different components of CAGE on the CLEVRER [73] dataset. As noted in Sec. 3.4, for ablations we train CAGE with a smaller batch size. However, later we show that the performance of the model scales accordingly with larger batch sizes.

In order to select the best configuration of the model, we assess its controllability in terms of scene composition. To this end, we have annotated 128 images from the test set of the CLEVRER dataset by selecting 4-6 random patches of the same object in an image. Then those patches are moved to a random location and the resulting scene is generated (see Fig. 4). The quality of the generated scenes is measured with a combination of two metrics: FID [30] for image realism and CTRL, which we propose for measuring control accuracy. CTRL is a ratio between S and D , where S is the cosine distance between normalized DINOv2 features of the original patches and the patches in the target location in the generated image and D is the cosine distance between normalized DINOv2 features of the original patches and the original patches in the generated image. Empirically we observed that both S and D are lower bounded by some positive number, which makes CTRL a valid metric. We test different configurations of the model and demonstrate that the model with 1 DINOv2 layer, $\pi = 0.1$, $k = 3$, with randomized t_i and scale/position invariance performs the best on CLEVRER among variants (see Tab. 1). Additionally we provide visual examples to highlight the limited control in the ablated models (see Fig. 4).

4.3 Quantitative Results

CLEVRER. Employing the optimal settings identified in the ablation studies, we train CAGE with the full batch size of 64 samples and report the results in Tab. 2. Besides the scene composition metrics studied in the ablations, following [16], we reconstruct 15 frames of a video from a single initial one conditioned on the control for the first generated frame. We report LPIPS [78], PSNR, SSIM [69] and FVD [65]. Table 2 shows that CAGE generates videos of better quality compared to prior work.

BAIR. Following prior work by Menapace *et al.* [53], we trained CAGE on the BAIR dataset [20]. We autoregressively generated 29 frames starting from a given initial frame and employing various controls. For feature extraction on BAIR we found that it is optimal to use the 2 last layers of ViT-B/14 variant of DINOv2. The experiment was conducted on the test videos from BAIR, utilizing an Euler solver with 50 steps as our ODE solver to ensure precise temporal evolution. We assessed the quality of the generated frames by reporting LPIPS [78] scores (between the generated images and

Table 1: Ablations of model components with respect to compositional scene generation quality. The controllability score (CTRL) and the image quality (FID) are evaluated. The row corresponding to the full model is highlighted in light-cyan. For the CTRL metric the average of 5 runs is reported.

l	π	k	random t_i	scale/pos inv.	CTRL \uparrow	FID \downarrow
1	0.1	3	✓		1.306	12.88
1	0.1	1	✓	✓	1.529	9.85
1	0.1	3		✓	<u>1.596</u>	5.82
1	0.9	3	✓	✓	1.464	6.19
1	0.5	3	✓	✓	1.566	5.19
1	0.01	3	✓	✓	0.782	6.11
4	0.1	3	✓	✓	1.084	5.24
2	0.1	3	✓	✓	1.500	4.95
1	0.1	3	✓	✓	1.615	<u>4.98</u>

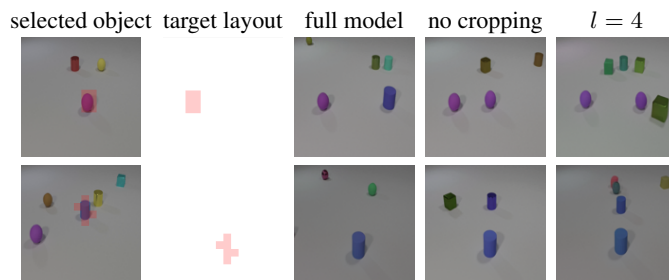


Fig. 4: Illustration of the effect of omitting calculation of the features on random crops (4th column) and using more DINOv2 layers (5th column). Those models tend to overfit to either position information or redundant texture information in the features, which results in limited controllability. In contrast to those models, the full model does not keep the moved object in the original location.

the ground truth frames) and FID [30] scores. More importantly, we utilized FVD [65] to quantify the quality of the generated motions and the consistency of the frames. To verify the generalization capability of our conditioning scheme, we evaluated the same model under three distinct settings (results shown in Tab. 3). In the 10% control setting, we encoded future frames using the same DINOv2 model employed during training and conditioned the model on 10% of these features, mirroring the training setting. To assess the robustness of our model, we also evaluated it with only 1% of the future features (1-2 features per frame on average), achieving superior FID and FVD scores compared to other models. Lastly, unlike the previous two settings, which were non-causal (i.e., conditioned on the features of the ground truth future frames), we experimented with a setting where features from the first frame were propagated to subsequent frames using the flow determined by assessing the cosine similarity between future patch features and the first frame’s features. We applied a high cosine similarity threshold of 0.95 to

Table 2: Evaluation of the generated videos on the *CLEVRER* dataset. 15 frames generated from a single initial frame. Control is only provided for the first generated frame.

Method	LPIPS↓	PSNR↑	SSIM↑	FID↓	FVD↓	CTRL↑
YODA [16]	0.126	30.07	0.93	5.7	70	-
CAGE (<i>ours</i>)	0.166	30.02	0.98	4.3	62	1.667

Table 3: Evaluation on the *BAIR* dataset.

Method	LPIPS↓	FID↓	FVD↓
MoCoGAN [64]	0.466	198.0	1380
MoCoGAN+ [53]	0.201	66.1	849
SAVP [44]	0.433	220.0	1720
SAVP+ [53]	0.154	27.2	303
CADDY [53]	0.202	35.9	423
Huang et al. [40]			
<i>positional</i>	0.202	28.5	333
<i>affine</i>	0.201	30.1	292
<i>non-param</i>	0.176	29.3	293
GLASS [15]	0.118	18.7	411
YODA [16]			
<i>5 controls</i>	<u>0.112</u>	18.2	264
<i>1 control</i>	0.142	19.2	339
CAGE (<i>ours</i>)			
<i>10% controls</i>	0.107	6.4	136
<i>1% controls</i>	0.149	<u>7.2</u>	<u>169</u>
<i>tracking</i>	0.194	9.1	214

Table 4: Optical flow error in pixels of the control applied to the robotic arm in the *BAIR* dataset. Average of 5 runs is reported.

Method	GT	from GT dist.	o.o.d.	
			S	L
CADDY [53]	6.29	-	-	-
GLASS [15]	1.75	25.00	25.07	30.06
YODA [16]	1.41	1.77	2.01	3.37
CAGE (<i>ours</i>)	2.74	2.93	3.57	5.45

Table 5: Evaluation of the generated videos on the *EPIC-KITCHENS* dataset.

Method	LPIPS↓	PSNR↑	FID↓	FVD↓
YODA [16]	0.436	16.22	152	664
CAGE (<i>ours</i>)	0.283	22.25	95	393

ensure the accuracy of the flows and maintain control percentage comparability with the training setting. This setting approximates the use of the model at inference, and the experiment shows that CAGE performs better than the prior work even under this domain gap between the training and the test times.

Even though methods with different controls are technically not comparable, other than for video quality, and different controllability metrics incorporate biases towards favoring certain controls, for completeness, we measure the controllability score proposed in [16] and report it in Tab. 4. This score measures the discrepancy in pixels between the intended control (which in [16] is an optical flow vector that is applied to an object) and the optical flow estimated with a pre-trained optical flow network (RAFT [62] in this case) between the initial and the generated frames. As done in the ablations, we annotate 128 frames from the *BAIR* dataset with the locations of the robot patches and apply random shifts to the patches to assess the controllability. Following [16], we report the controllability score in 4 different settings: 1) the shift is estimated from the ground truth future frame 2) the shift is generated with a uniform direction and the norm sampled from the ground truth distribution, which is $\mathcal{N}(7.19, 5.12)$ 3) o.o.d. S - the same as 2), but the norm comes from $\mathcal{N}(10, 0.1)$ 4) o.o.d. L - the same as 2), but the norm comes from $\mathcal{N}(20, 0.1)$. CAGE performs slightly worse than [16]

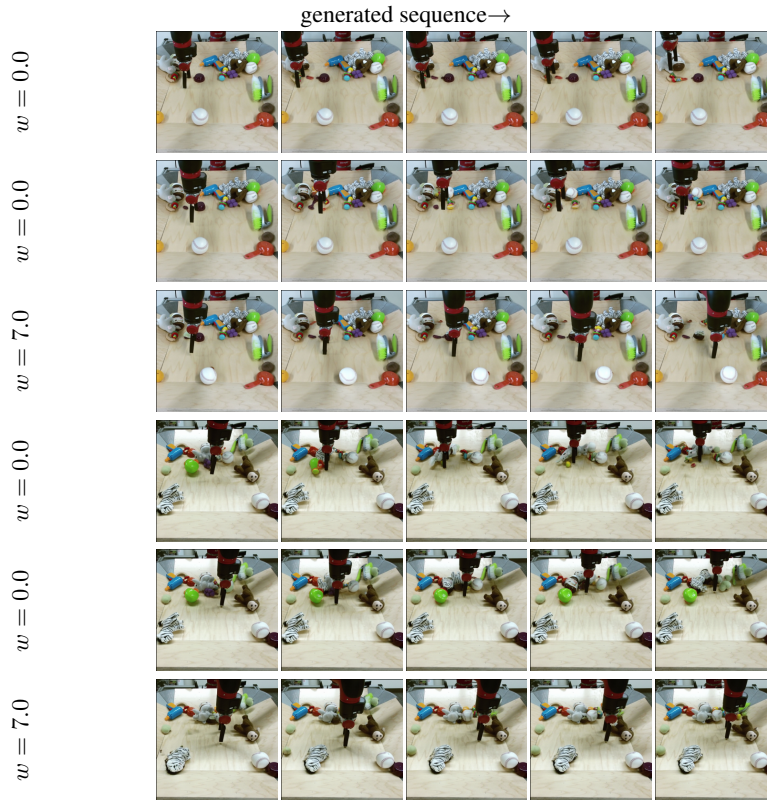


Fig. 5: The effect of CFG strength on the generalization to out of distribution controls on the BAIR dataset. While the robotic arm can be controlled with no guidance ($w = 0.0$), with larger w the model is also able to move the background objects that do not move on their own in the training videos. Click on the images in the first column to play them as videos in Acrobat Reader.

in this experiment, but it is worth noting that this metric is measured in pixels, while our method works with patches that lie on a fixed grid. Nevertheless, the highest score of CAGE, which is 5.45, is smaller than half the patch size, which is 16×16 . Based on that we can claim the controllability of our method.

EPIC-KITCHENS. We perform the same reconstruction experiment as before for the EPIC-KITCHENS dataset to show that our model works in even more realistic settings. We use the model configuration from BAIR and autoregressively generated 15 frames from 1 conditioned on controls estimated from the future ground truth frames. We also trained YODA [16] on the same data using the official codebase⁴ and evaluated it the same way. The results are in Tab. 5.

⁴ <https://github.com/araachie/yoda>

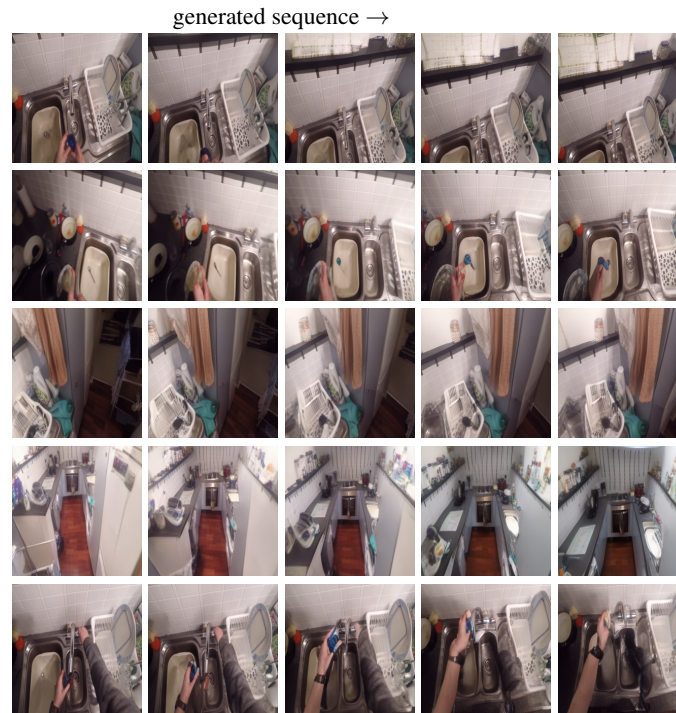


Fig. 6: Generated videos on the EPIC-KITCHENS dataset. CAGE is able to model such motions as ego-motion or the movement of the hands. The controls are superimposed with the images in the first column. Click on the images in the first column to play them as videos in Acrobat Reader. Notice that the blue arrows are shown only to illustrate the intended motion and are not part of the control signal, which consists only of features from the selected patches that are moved in the direction pointed with the blue arrows.

4.4 Qualitative Results

In this section we show some qualitative results to visually illustrate various capabilities of CAGE (more, including videos, can be found in the supplementary).

The main contribution of our model is the ability to both compose and animate scenes using a unified control. This is demonstrated in Fig. 1. With the trained model one is able to select object patches from different images and compose them into a unique scene. This is achieved by extracting the DINOv2 features from the selected patches and placing them in the indicated locations to form the control that is fed to the model. Additionally, one may also specify the motion of the objects by moving the patches in the future frames. CAGE carefully adjusts the appearance of the objects to the locations of the features in the control map, while preserving the objects’ identities.

Figure 5 depicts some out of distribution controls on BAIR. As previously discussed, using larger w in classifier-free guidance allows us to adapt to o.o.d. control, such as moving background objects in BAIR.

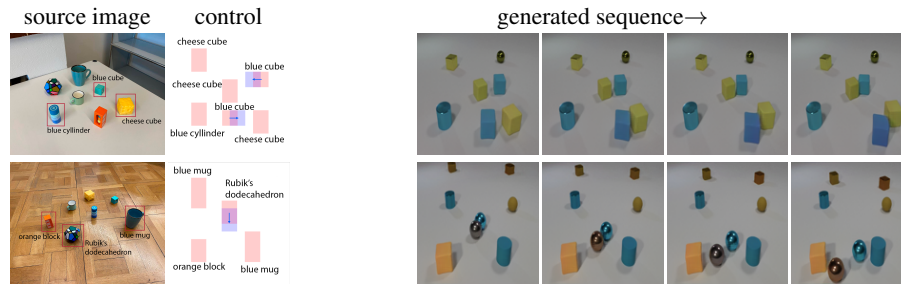


Fig. 7: Examples of cross-domain transfer. The features of the objects from images in the first column are borrowed to compose and animate the scenes in the CLEVRER dataset. Two different configurations of the same set of objects on different backgrounds are shown. Notice how CAGE resolves the domain gap and performs a reasonable transfer of the objects (in terms of shapes and colors). However some objects with irregular shape and texture, such as the Rubik’s dodecahedron, may turn to multiple objects when transferred. Click on the first images in the generated sequences to play them as videos in Acrobat Reader.

In Fig. 6 we show examples of videos generated under different control scenarios, including camera and hand motion.

Finally, in Fig. 7 we demonstrate the capability of the model to generalize to cross-domain scenarios. We select the features for control from images from a different domain and transfer them to the data domain the model was trained on (e.g. real objects to CLEVRER objects). This is possible because of our specific choice of conditioning the generation on DINOv2 features that were trained on a large open image dataset and hence are abstract and data-agnostic.

5 Conclusion and Limitations

In this paper we introduced CAGE, an unsupervised method for controllable video generation through scene composition and animation. CAGE is able to compose scenes of objects adopted from other frames, including out of domain images, and to animate them. This is achieved by conditioning the generation on a sparse set of DINOv2 spatial tokens that describe the appearance of the objects as well as their location in space and time. We also proposed a procedure to calculate the features in such a way that the model becomes invariant to the position and the scale of the source object. We conducted a series of experiments to demonstrate the capabilities and the controllability of our method. However, the fact that the DINOv2 features are calculated on a fixed grid of patches provides some room for improving the accuracy of the control. In theory this can be achieved by interpolating the internal position encoding of DINOv2 patches. We leave this for future exploration.

Acknowledgements. This work was supported by grant 188690 of the Swiss National Science Foundation.

	EPIC-KITCHENS 256 × 256 [13]
embed_dim	8
n_embed	16384
double_z	False
z_channels	8
resolution	256
in_channels	3
out_ch	3
ch	128
ch_mult	[1,1,2,2,4]
num_res_blocks	2
attn_resolutions	[16]
dropout	0.0
disc_conditional	False
disc_in_channels	3
disc_start	20k
disc_weight	0.8
codebook_weight	1.0

Table 6: Training configuration of VQGAN [22] for the EPIC-KITCHENS [13] dataset.

A Additional Details

Training. Following [58], we train CAGE in the latent space of pretrained VQGAN [22] models. For the BAIR [20] and CLEVRER [73] datasets we used the pretrained autoencoders from the official repository of YODA [16]⁵. For the EPIC-KITCHENS [13] dataset, we trained the autoencoder using the official implementation of VQGAN⁶. The training specifications of VQGAN can be found in Tab. 6. The model for the EPIC-KITCHENS dataset was trained on a single kitchen/person, namely P03. We used 49 videos for training and left out 1 video (P03_28) for the testing purposes.

Inference. Once the model is trained, we generate videos in an autoregressive manner, subsequently denoising windows of future frames conditioned on previously generated ones. In order to generate the current window, one needs to start by sampling a noise tensor from the standard normal distribution and then integrate the flow ODE from 0 to 1 using a numerical ODE solver (we used the `euler` solver with 20-40 steps).

B Additional Qualitative Results

In this section we provide more videos generated with CAGE. All the results in the main paper and this supplementary material are obtained using images from the test sets of the corresponding datasets, *i.e.* unseen during training. The results can also be viewed on the project’s website⁷. The figures in this pdf on the other hand show the quality of separate frames that cannot be assessed with the gifs from the webpage.

⁵ <https://github.com/araachie/yoda>

⁶ <https://github.com/CompVis/taming-transformers>

⁷ <https://araachie.github.io/cage>

Composition and Animation. Figure 8 shows additional examples of videos generated with CAGE by composing scenes from object features adopted from other images.

Out of Distribution Controls. In the main paper we show the generalization capabilities of CAGE to o.o.d. controls in the BAIR [20] dataset, such as moving background objects. Here we additionally provide videos generated from o.o.d. controls in the CLEVRER [73] dataset (see Fig. 9). These controls include curved trajectories and sudden direction and velocity changes (*e.g.* moving back and stopping).

Comparison to Prior Work. In the main paper we provided some quantitative comparisons to prior work. Here we accomplish this by visually comparing the videos generated with our method to those generated with YODA [16] (see Fig. 10) on the EPIC-KITCHENS [13] dataset. Notice that our model generates more temporally-consistent and realistic videos, while accurately following the control.

Cross-domain Transfer. Thanks to the use of DINOv2 [56] features for conditioning, at inference our model is able to compose scenes from features adopted from out of domain images in a zero-shot manner. In the main paper we provided examples of this emerging capability of CAGE on the CLEVRER [73] dataset. Here we demonstrate that this capability also extends to more complex data, such as transferring from other robotic scenes from the ROBONET [14] dataset to BAIR, or using features from other kitchens in the EPIC-KITCHENS [13] dataset to compose and animate scenes in the kitchen the model was trained on (see Fig. 11).

Long Video Generation. To demonstrate controllability of our method we opted for generating short videos, so that one is able to follow the objects and compare their motion to the control signal. However, this might have caused an impression that our model is only able to generate short videos. In order to address this issue, we provide some extremely long (512 frames) videos generated with CAGE on the CLEVRER [73] dataset. In order not to overload the PDF, we only provide the videos via the webpage (check the “Long Video Generation” section on the project’s website). Despite the fact that CAGE was only trained on short (3 frames) windows, long video generation is possible with our method, as it correlates subsequent windows of frames via conditioning on the reference and the context frames. Thus, CAGE can qualify as an autoregressive model.

Robustness to the Number of Controls. In Fig. 12 we show some generated sequences with only one vs many DINOv2 [56] tokens provided per object. While CAGE is pretty robust to the number of controls provided and can inpaint the missing information, the sequences generated conditioned on more tokens are more consistent with the source image (*e.g.* in the last video the blue cube does not rotate with more tokens provided, *i.e.* the pose of the object is fixed given the features).

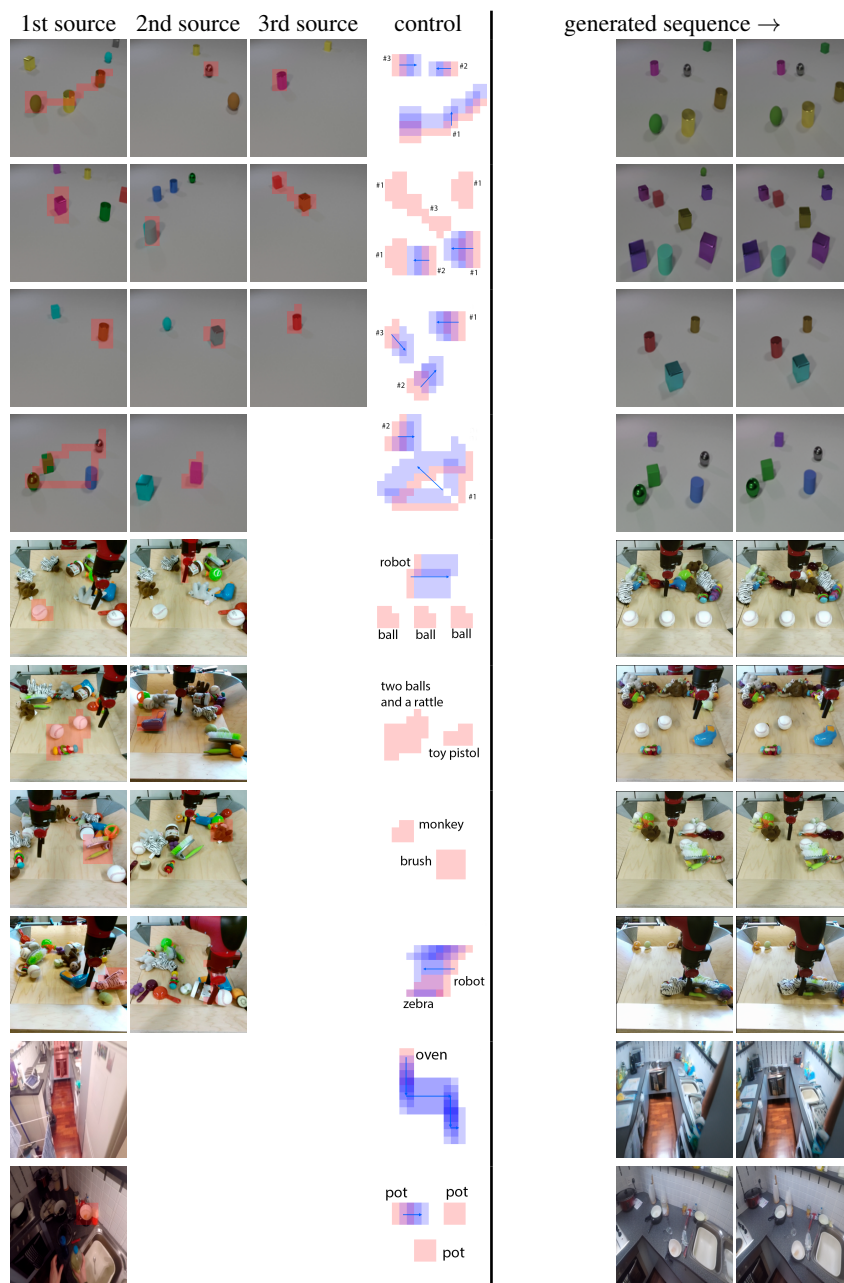


Fig. 8: Composition and animation with CAGE on different datasets. Red patches correspond to the copied features from the source images. Blue patches correspond to the intended future locations of the red patches. Blue arrows only illustrate the direction of the motion, but are not used as conditioning signals in the model. Click on the first generated images to play them as videos in Acrobat Reader.

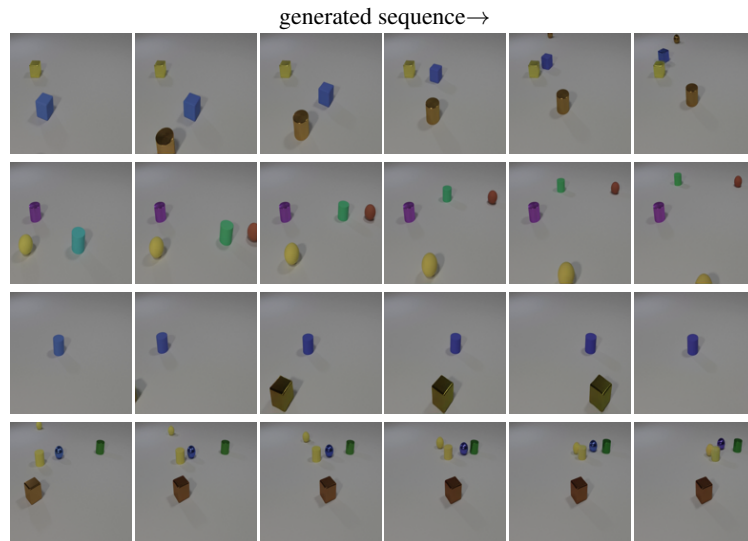


Fig. 9: Generalization to o.o.d. controls on the CLEVRER [73] dataset. Click on the images in the first column to play them as videos in Acrobat Reader.

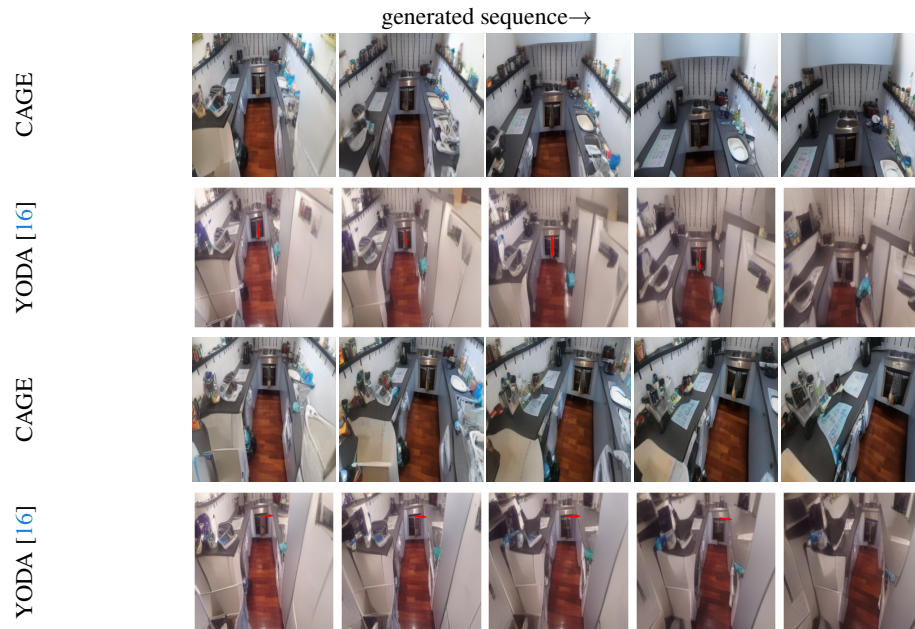


Fig. 10: Comparison to YODA [16] on controllable video generation on the EPIC-KITCHENS [13] dataset. CAGE generates more realistic sequences, while following the control. Click on the images in the first column to play them as videos in Acrobat Reader.

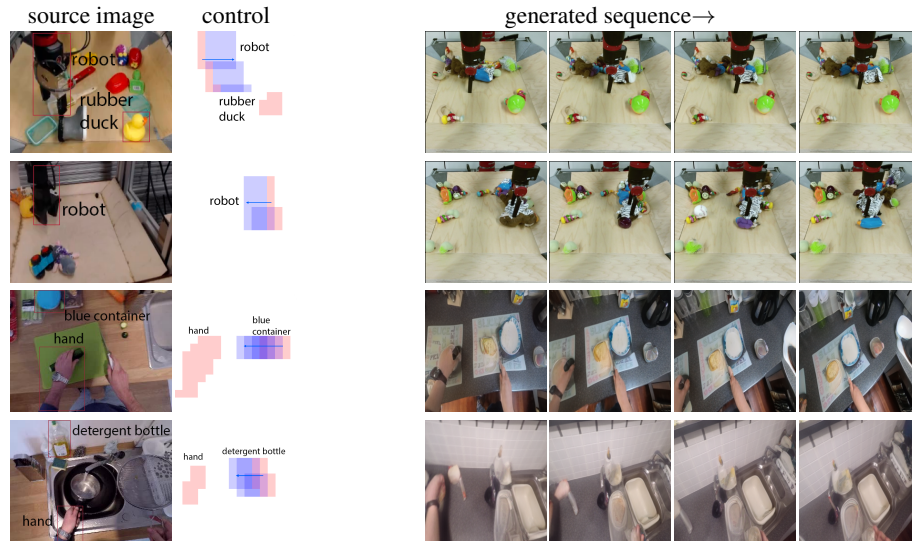


Fig. 11: Examples of cross-domain transfer on the BAIR [20] and the EPIC-KITCHENS [13] datasets. Notice how CAGE changes the appearances of the objects when transferring them to the familiar domain (*e.g.* the color of the watch on the hand). Click on the first images in the generated sequences to play them as videos in Acrobat Reader.

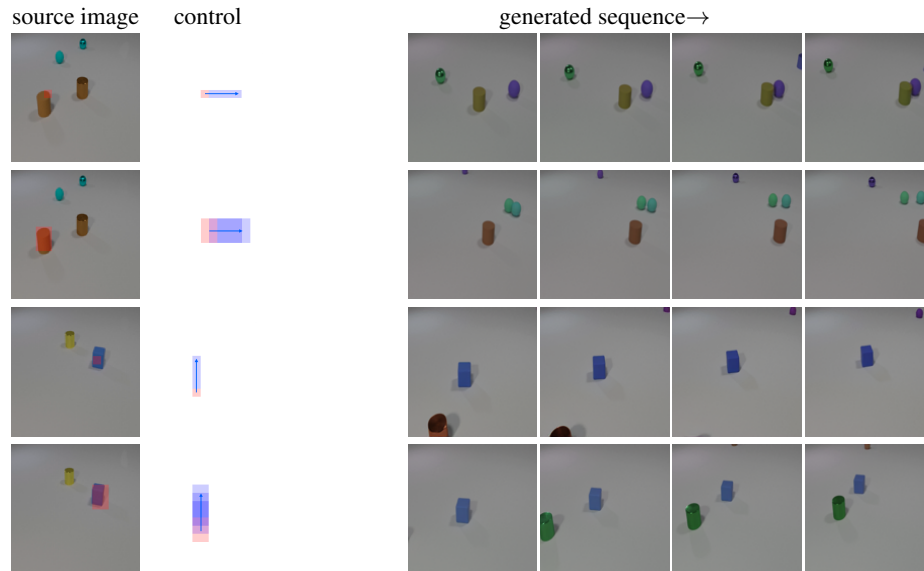


Fig. 12: The effect of the number of control tokens on the generated sequences. More tokens make the generated object more consistent with the source appearance (*e.g.* in color and pose). Click on the first images in the generated sequences to play them as videos in Acrobat Reader.

References

1. Bielski, A., Favaro, P.: Move: Unsupervised movable object segmentation and detection. ArXiv **abs/2210.07920** (2022), <https://api.semanticscholar.org/CorpusID:252907913>
2. Blattmann, A., Milbich, T., Dorkenwald, M., Ommer, B.: ipoke: Poking a still image for controlled stochastic video synthesis. 2021 IEEE/CVF International Conference on Computer Vision (ICCV) pp. 14687–14697 (2021), <https://api.semanticscholar.org/CorpusID:235743021>
3. Blattmann, A., Dockhorn, T., Kulal, S., Mendeleevitch, D., Kilian, M., Lorenz, D., Levi, Y., English, Z., Voleti, V., Letts, A., et al.: Stable video diffusion: Scaling latent video diffusion models to large datasets. arXiv preprint arXiv:2311.15127 (2023)
4. Blattmann, A., Milbich, T., Dorkenwald, M., Ommer, B.: ipoke: Poking a still image for controlled stochastic video synthesis. In: Proceedings of the IEEE/CVF International Conference on Computer Vision. pp. 14707–14717 (2021)
5. Bruce, J., Dennis, M., Edwards, A., Parker-Holder, J., Shi, Y., Hughes, E., Lai, M., Mavalankar, A., Steigerwald, R., Apps, C., et al.: Genie: Generative interactive environments. arXiv preprint arXiv:2402.15391 (2024)
6. Caron, M., Misra, I., Mairal, J., Goyal, P., Bojanowski, P., Joulin, A.: Unsupervised learning of visual features by contrasting cluster assignments. *Advances in neural information processing systems* **33**, 9912–9924 (2020)
7. Caron, M., Touvron, H., Misra, I., Jégou, H., Mairal, J., Bojanowski, P., Joulin, A.: Emerging properties in self-supervised vision transformers. In: Proceedings of the International Conference on Computer Vision (ICCV) (2021)
8. Casanova, A., Careil, M., Verbeek, J., Drozdal, M., Romero-Soriano, A.: Instance-conditioned gan. In: Neural Information Processing Systems (2021), <https://api.semanticscholar.org/CorpusID:237491885>
9. Chen, C., Shu, J., Chen, L., He, G., Wang, C., Li, Y.: Motion-zero: Zero-shot moving object control framework for diffusion-based video generation. ArXiv **abs/2401.10150** (2024), <https://api.semanticscholar.org/CorpusID:267035012>
10. Chen, T., Kornblith, S., Norouzi, M., Hinton, G.E.: A simple framework for contrastive learning of visual representations. ArXiv **abs/2002.05709** (2020), <https://api.semanticscholar.org/CorpusID:211096730>
11. Chen, W., Wu, J., Xie, P., Wu, H., Li, J., Xia, X., Xiao, X., Lin, L.J.: Control-a-video: Controllable text-to-video generation with diffusion models. ArXiv **abs/2305.13840** (2023), <https://api.semanticscholar.org/CorpusID:258841645>
12. Chen, X., Fan, H., Girshick, R.B., He, K.: Improved baselines with momentum contrastive learning. ArXiv **abs/2003.04297** (2020), <https://api.semanticscholar.org/CorpusID:212633993>
13. Damen, D., Doughty, H., Farinella, G.M., Fidler, S., Furnari, A., Kazakos, E., Moltisanti, D., Munro, J., Perrett, T., Price, W., Wray, M.: The epic-kitchens dataset: Collection, challenges and baselines. *IEEE Transactions on Pattern Analysis and Machine Intelligence (TPAMI)* **43**(11), 4125–4141 (2021). <https://doi.org/10.1109/TPAMI.2020.2991965>
14. Dasari, S., Ebert, F., Tian, S., Nair, S., Bucher, B., Schmeckpeper, K., Singh, S., Levine, S., Finn, C.: Robonet: Large-scale multi-robot learning. arXiv preprint arXiv:1910.11215 (2019)
15. Davtyan, A., Favaro, P.: Controllable video generation through global and local motion dynamics. In: Avidan, S., Brostow, G., Cissé, M., Farinella, G.M., Hassner, T. (eds.) *Computer Vision – ECCV 2022*. pp. 68–84. Springer Nature Switzerland, Cham (2022)

16. Davtyan, A., Favaro, P.: Learn the force we can: Enabling sparse motion control in multi-object video generation (2024)
17. Davtyan, A., Sameni, S., Favaro, P.: Efficient video prediction via sparsely conditioned flow matching. In: Proceedings of the IEEE/CVF International Conference on Computer Vision (ICCV). pp. 23263–23274 (October 2023)
18. Dhariwal, P., Nichol, A.: Diffusion models beat gans on image synthesis. *Advances in neural information processing systems* **34**, 8780–8794 (2021)
19. Dosovitskiy, A., Beyer, L., Kolesnikov, A., Weissenborn, D., Zhai, X., Unterthiner, T., Dehghani, M., Minderer, M., Heigold, G., Gelly, S., Uszkoreit, J., Houlsby, N.: An image is worth 16x16 words: Transformers for image recognition at scale. *ArXiv abs/2010.11929* (2020), <https://api.semanticscholar.org/CorpusID:225039882>
20. Ebert, F., Finn, C., Lee, A.X., Levine, S.: Self-supervised visual planning with temporal skip connections. In: *CoRL* (2017)
21. Epstein, D., Park, T., Zhang, R., Shechtman, E., Efros, A.A.: Blobgan: Spatially disentangled scene representations. *ArXiv abs/2205.02837* (2022), <https://api.semanticscholar.org/CorpusID:248524853>
22. Esser, P., Rombach, R., Ommer, B.: Taming transformers for high-resolution image synthesis. In: Proceedings of the IEEE/CVF conference on computer vision and pattern recognition. pp. 12873–12883 (2021)
23. Guo, H., Wu, F., Qin, Y., Li, R., Li, K., Li, K.: Recent trends in task and motion planning for robotics: A survey. *ACM Comput. Surv.* **55**(13s) (jul 2023). <https://doi.org/10.1145/3583136>, <https://doi.org/10.1145/3583136>
24. Guo, Y., Yang, C., Rao, A., Wang, Y., Qiao, Y., Lin, D., Dai, B.: Animatediff: Animate your personalized text-to-image diffusion models without specific tuning. *arXiv preprint arXiv:2307.04725* (2023)
25. Ha, D., Schmidhuber, J.: Recurrent world models facilitate policy evolution. In: *Advances in Neural Information Processing Systems 31*, pp. 2451–2463. Curran Associates, Inc. (2018), <https://papers.nips.cc/paper/7512-recurrent-world-models-facilitate-policy-evolution>, <https://worldmodels.github.io>
26. Handa, A., Allshire, A., Makoviychuk, V., Petrenko, A., Singh, R., Liu, J., Makoviichuk, D., Wyk, K.V., Zhurkevich, A., Sundaralingam, B., Narang, Y., Lafleche, J.F., Fox, D., State, G.: Dextreme: Transfer of agile in-hand manipulation from simulation to reality. In: *ICRA* (2023)
27. Hao, Z., Huang, X., Belongie, S.: Controllable video generation with sparse trajectories. In: Proceedings of the IEEE Conference on Computer Vision and Pattern Recognition. pp. 7854–7863 (2018)
28. Hatamizadeh, A., Song, J., Liu, G., Kautz, J., Vahdat, A.: Diffit: Diffusion vision transformers for image generation. *ArXiv abs/2312.02139* (2023), <https://api.semanticscholar.org/CorpusID:265609345>
29. He, K., Chen, X., Xie, S., Li, Y., Doll’ar, P., Girshick, R.B.: Masked autoencoders are scalable vision learners. *2022 IEEE/CVF Conference on Computer Vision and Pattern Recognition (CVPR)* pp. 15979–15988 (2021), <https://api.semanticscholar.org/CorpusID:243985980>
30. Heusel, M., Ramsauer, H., Unterthiner, T., Nessler, B., Hochreiter, S.: Gans trained by a two time-scale update rule converge to a local nash equilibrium. *Advances in neural information processing systems* **30** (2017)
31. Ho, J., Chan, W., Saharia, C., Whang, J., Gao, R., Gritsenko, A., Kingma, D.P., Poole, B., Norouzi, M., Fleet, D.J., et al.: Imagen video: High definition video generation with diffusion models. *arXiv preprint arXiv:2210.02303* (2022)
32. Ho, J., Jain, A., Abbeel, P.: Denoising diffusion probabilistic models. *Advances in neural information processing systems* **33**, 6840–6851 (2020)

33. Ho, J., Salimans, T.: Classifier-free diffusion guidance. arXiv preprint arXiv:2207.12598 (2022)
34. Ho, J., Salimans, T., Gritsenko, A., Chan, W., Norouzi, M., Fleet, D.J.: Video diffusion models. arXiv preprint arXiv:2204.03458 (2022)
35. Hoppe, T., Mehrjou, A., Bauer, S., Nielsen, D., Dittadi, A.: Diffusion models for video prediction and infilling. *Trans. Mach. Learn. Res.* **2022** (2022), <https://api.semanticscholar.org/CorpusID:249674747>
36. Hu, A., Russell, L., Yeo, H., Murez, Z., Fedoseev, G., Kendall, A., Shotton, J., Corrado, G.: Gaia-1: A generative world model for autonomous driving (2023)
37. Hu, V.T., Chen, Y., Caron, M., Asano, Y.M., Snoek, C.G.M., Ommer, B.: Guided diffusion from self-supervised diffusion features. *ArXiv abs/2312.08825* (2023), <https://api.semanticscholar.org/CorpusID:266210467>
38. Hu, Y., Luo, C., Chen, Z.: Make it move: Controllable image-to-video generation with text descriptions. 2022 IEEE/CVF Conference on Computer Vision and Pattern Recognition (CVPR) pp. 18198–18207 (2021), <https://api.semanticscholar.org/CorpusID:244908665>
39. Huang, H.P., Su, Y.C., Sun, D., Jiang, L., Jia, X., Zhu, Y., Yang, M.H.: Fine-grained controllable video generation via object appearance and context. *ArXiv abs/2312.02919* (2023), <https://api.semanticscholar.org/CorpusID:265658916>
40. Huang, J., Jin, Y., Yi, K.M., Sigal, L.: Layered controllable video generation. In: Avidan, S., Brostow, G., Cissé, M., Farinella, G.M., Hassner, T. (eds.) *Computer Vision – ECCV 2022*. pp. 546–564. Springer Nature Switzerland, Cham (2022)
41. Huang, S., Dossa, R.F.J., Ye, C., Braga, J., Chakraborty, D., Mehta, K., Araújo, J.G.: Cleanrl: High-quality single-file implementations of deep reinforcement learning algorithms. *Journal of Machine Learning Research* **23**(274), 1–18 (2022), <http://jmlr.org/papers/v23/21-1342.html>
42. Hudson, D.A., Zitnick, C.L.: Compositional transformers for scene generation. In: *Neural Information Processing Systems* (2021), <https://api.semanticscholar.org/CorpusID:244270383>
43. LeCun, Y.: A path towards autonomous machine intelligence. In: arXiv preprint (2022)
44. Lee, A.X., Zhang, R., Ebert, F., Abbeel, P., Finn, C., Levine, S.: Stochastic adversarial video prediction. arXiv preprint arXiv:1804.01523 (2018)
45. Li, T., Katabi, D., He, K.: Self-conditioned image generation via generating representations. *ArXiv abs/2312.03701* (2023), <https://api.semanticscholar.org/CorpusID:265664611>
46. Lipman, Y., Chen, R.T., Ben-Hamu, H., Nickel, M., Le, M.: Flow matching for generative modeling. arXiv preprint arXiv:2210.02747 (2022)
47. Liu, X., Gong, C., Liu, Q.: Flow straight and fast: Learning to generate and transfer data with rectified flow. arXiv preprint arXiv:2209.03003 (2022)
48. Loshchilov, I., Hutter, F.: Decoupled weight decay regularization. In: *International Conference on Learning Representations* (2017), <https://api.semanticscholar.org/CorpusID:53592270>
49. Ma, W.D.K., Lewis, J.P., Kleijn, W.: Trailblazer: Trajectory control for diffusion-based video generation. *ArXiv abs/2401.00896* (2023), <https://api.semanticscholar.org/CorpusID:266725649>
50. Ma, Y., Cun, X., He, Y.Y., Qi, C., Wang, X., Shan, Y., Li, X., Chen, Q.: Magicstick: Controllable video editing via control handle transformations. *ArXiv abs/2312.03047* (2023), <https://api.semanticscholar.org/CorpusID:265693920>
51. Makovychuk, V., Wawrzyniak, L., Guo, Y., Lu, M., Storey, K., Macklin, M., Hoeller, D., Rudin, N., Allshire, A., Handa, A., State, G.: Isaac gym: High performance gpu-based physics simulation for robot learning (2021)

52. Menapace, W., Lathuiliere, S., Siarohin, A., Theobalt, C., Tulyakov, S., Golyanik, V., Ricci, E.: Playable environments: Video manipulation in space and time. In: Proceedings of the IEEE/CVF Conference on Computer Vision and Pattern Recognition. pp. 3584–3593 (2022)
53. Menapace, W., Lathuilière, S., Tulyakov, S., Siarohin, A., Ricci, E.: Playable video generation. In: Proceedings of the IEEE/CVF Conference on Computer Vision and Pattern Recognition. pp. 10061–10070 (2021)
54. Niemeyer, M., Geiger, A.: Giraffe: Representing scenes as compositional generative neural feature fields. 2021 IEEE/CVF Conference on Computer Vision and Pattern Recognition (CVPR) pp. 11448–11459 (2020), <https://api.semanticscholar.org/CorpusID:227151657>
55. van den Oord, A., Li, Y., Vinyals, O.: Representation learning with contrastive predictive coding. ArXiv [abs/1807.03748](https://arxiv.org/abs/1807.03748) (2018), <https://api.semanticscholar.org/CorpusID:49670925>
56. Oquab, M., Darcet, T., Moutakanni, T., Vo, H.Q., Szafraniec, M., Khalidov, V., Fernandez, P., Haziza, D., Massa, F., El-Nouby, A., Assran, M., Ballas, N., Galuba, W., Howes, R., Huang, P.Y.B., Li, S.W., Misra, I., Rabbat, M.G., Sharma, V., Synnaeve, G., Xu, H., Jégou, H., Mairal, J., Labatut, P., Joulin, A., Bojanowski, P.: Dinov2: Learning robust visual features without supervision. ArXiv [abs/2304.07193](https://arxiv.org/abs/2304.07193) (2023), <https://api.semanticscholar.org/CorpusID:258170077>
57. Peng, X.B., Ma, Z., Abbeel, P., Levine, S., Kanazawa, A.: Amp: Adversarial motion priors for stylized physics-based character control. ACM Trans. Graph. **40**(4) (Jul 2021). <https://doi.org/10.1145/3450626.3459670>, <http://doi.acm.org/10.1145/3450626.3459670>
58. Rombach, R., Blattmann, A., Lorenz, D., Esser, P., Ommer, B.: High-resolution image synthesis with latent diffusion models. In: Proceedings of the IEEE/CVF Conference on Computer Vision and Pattern Recognition. pp. 10684–10695 (2022)
59. Ruhe, D., Heek, J., Salimans, T., Hoogeboom, E.: Rolling diffusion models. arXiv preprint [arXiv:2402.09470](https://arxiv.org/abs/2402.09470) (2024)
60. Shi, X., Huang, Z., Wang, F.Y., Bian, W., Li, D., Zhang, Y., Zhang, M., Cheung, K.C., See, S., Qin, H., Da, J., Li, H.: Motion-i2v: Consistent and controllable image-to-video generation with explicit motion modeling. ArXiv [abs/2401.15977](https://arxiv.org/abs/2401.15977) (2024), <https://api.semanticscholar.org/CorpusID:267311454>
61. Song, J., Meng, C., Ermon, S.: Denoising diffusion implicit models. arXiv preprint [arXiv:2010.02502](https://arxiv.org/abs/2010.02502) (2020)
62. Teed, Z., Deng, J.: Raft: Recurrent all-pairs field transforms for optical flow. In: Computer Vision–ECCV 2020: 16th European Conference, Glasgow, UK, August 23–28, 2020, Proceedings, Part II 16. pp. 402–419. Springer (2020)
63. Tong, Z., Song, Y., Wang, J., Wang, L.: Videomae: Masked autoencoders are data-efficient learners for self-supervised video pre-training. ArXiv [abs/2203.12602](https://arxiv.org/abs/2203.12602) (2022), <https://api.semanticscholar.org/CorpusID:247619234>
64. Tulyakov, S., Liu, M.Y., Yang, X., Kautz, J.: Mocogan: Decomposing motion and content for video generation. In: Proceedings of the IEEE conference on computer vision and pattern recognition. pp. 1526–1535 (2018)
65. Unterthiner, T., van Steenkiste, S., Kurach, K., Marinier, R., Michalski, M., Gelly, S.: Towards accurate generative models of video: A new metric & challenges. ArXiv [abs/1812.01717](https://arxiv.org/abs/1812.01717) (2018), <https://api.semanticscholar.org/CorpusID:54458806>
66. Vaswani, A., Shazeer, N.M., Parmar, N., Uszkoreit, J., Jones, L., Gomez, A.N., Kaiser, L., Polosukhin, I.: Attention is all you need. In: Neural Information Processing Systems (2017), <https://api.semanticscholar.org/CorpusID:13756489>

67. Voleti, V.S., Jolicoeur-Martineau, A., Pal, C.J.: Mcvd: Masked conditional video diffusion for prediction, generation, and interpolation. ArXiv **abs/2205.09853** (2022), <https://api.semanticscholar.org/CorpusID:248965384>
68. Wang, J., Zhang, Y., Zou, J., Zeng, Y., Wei, G., Yuan, L., Li, H.: Boximator: Generating rich and controllable motions for video synthesis. ArXiv **abs/2402.01566** (2024), <https://api.semanticscholar.org/CorpusID:267406297>
69. Wang, Z., Bovik, A.C., Sheikh, H.R., Simoncelli, E.P.: Image quality assessment: from error visibility to structural similarity. *IEEE transactions on image processing* **13**(4), 600–612 (2004)
70. Wu, K., Peng, H., Chen, M., Fu, J., Chao, H.: Rethinking and improving relative position encoding for vision transformer. 2021 IEEE/CVF International Conference on Computer Vision (ICCV) pp. 10013–10021 (2021), <https://api.semanticscholar.org/CorpusID:236493453>
71. Yang, J., Ivanovic, B., Litany, O., Weng, X., Kim, S.W., Li, B., Che, T., Xu, D., Fidler, S., Pavone, M., Wang, Y.: Emernerf: Emergent spatial-temporal scene decomposition via self-supervision. ArXiv **abs/2311.02077** (2023), <https://api.semanticscholar.org/CorpusID:265019040>
72. Yang, J., Luo, K.Z., Li, J., Weinberger, K.Q., Tian, Y., Wang, Y.: Denoising vision transformers. ArXiv **abs/2401.02957** (2024), <https://api.semanticscholar.org/CorpusID:266818138>
73. Yi, K., Gan, C., Li, Y., Kohli, P., Wu, J., Torralba, A., Tenenbaum, J.B.: Clevrer: Collision events for video representation and reasoning. ArXiv **abs/1910.01442** (2019), <https://api.semanticscholar.org/CorpusID:203641884>
74. Zhang, D.J., Li, D., Le, H., Shou, M.Z., Xiong, C., Sahoo, D.: Moonshot: Towards controllable video generation and editing with multimodal conditions. ArXiv **abs/2401.01827** (2024), <https://api.semanticscholar.org/CorpusID:266741873>
75. Zhang, D.J., Wu, J.Z., Liu, J.W., Zhao, R., Ran, L., Gu, Y., Gao, D., Shou, M.Z.: Show-1: Marrying pixel and latent diffusion models for text-to-video generation. arXiv preprint arXiv:2309.15818 (2023)
76. Zhang, L., Xiong, Y., Yang, Z., Casas, S., Hu, R., Urtasun, R.: Learning unsupervised world models for autonomous driving via discrete diffusion. In: The Twelfth International Conference on Learning Representations (2024), <https://openreview.net/forum?id=Ps175UCoZM>
77. Zhang, L., Rao, A., Agrawala, M.: Adding conditional control to text-to-image diffusion models. 2023 IEEE/CVF International Conference on Computer Vision (ICCV) pp. 3813–3824 (2023), <https://api.semanticscholar.org/CorpusID:256827727>
78. Zhang, R., Isola, P., Efros, A.A., Shechtman, E., Wang, O.: The unreasonable effectiveness of deep features as a perceptual metric. In: Proceedings of the IEEE conference on computer vision and pattern recognition. pp. 586–595 (2018)
79. Zhang, Y., Wei, Y., Jiang, D., Zhang, X., Zuo, W., Tian, Q.: Controlvideo: Training-free controllable text-to-video generation. ArXiv **abs/2305.13077** (2023), <https://api.semanticscholar.org/CorpusID:258832670>
80. Zhang, Z., Liu, R., Aberman, K., Hanocka, R.: Tedi: Temporally-entangled diffusion for long-term motion synthesis. arXiv preprint arXiv:2307.15042 (2023)